
University of Groningen
**Zernike Institute for Advanced Materials**

Top Master Nanoscience Thesis

# Towards the Understanding of 3-terminal Metallic Spintronics Devices

Written by

**Nilesh Awari**

Top Master Nanoscience Cohort 2012-2014

Supervisors

**prof. dr. ir. B. J. van Wees**

**F. K. Dejene**

Physics of Nanodevices

Submitted on

**July 18, 2014**

Referent

**prof. dr. J. Ye**

# Abstract

Injection of spins into a non-magnetic metal (NM) including semiconductors is essential step towards the integrating the spin degree of freedom of an electron into the conventional electronics. To achieve the higher spin injection efficiency an insulation layer is inserted between ferromagnet (FM) and NM. In order to understand the spin injection in a better way it is therefore required to distinguish between the electrically driven spin signals and the impurity assisted effects in the tunnel barrier.

Here we fabricate a 3-terminal spintronics devices using permaolly (Py) and cobalt (Co) as a FM and Al as a NM materials. The fabricated devices are studied for their non-linear I-V curves and the change in the junction resistance as a function of applied in-plane and out of plane magnetization (Inverted Hanle effect and Hanle effect). The spin accumulation of 8 orders of higher magnitude than expected from the standard theory of the spin injection is observed. The finite element model was used to calculate the spin accumulation based on the standard theory of the spin injection. An explanation for this very high observed spin accumulation is given based on the impurity assisted tunneling. This tunneling, in externally applied magnetic field, shows the magneto-resistance effect. This magneto resistance effect shows that the tunneling current through impurity states in tunnel junction can be modulated in external magnetic field.

# Contents


1 Introduction 6
- 1.1 Concept of spin injection and relaxation 7
- 1.2 Non-local 4 terminal geometry 8
- 1.3 Local 3-terminal geometry 9

2 Theoretical Background 12
- 2.1 The two channel model 12
- 2.2 Finite element modelling 13
- 2.3 Simmons model 15
- 2.4 Hanle effect and impact of interface roughness and in-plane external magnetic field on it 17

3 Experimental Section 21
- 3.1 Fabrication details 21
- 3.2 Measurement setups and techniques 25

4 Results and analysis 27

5 Conclusion 35

6 Acknowledgements 36

7 References 37

# Chapter 1: Introduction

The long sought goal of electronics is to improve the functionality of modern electrical devices for wide range of applications. Improved functionality of such devices with decreasing dimensions is limited by the physical limits on device dimensions. To overcome this challenge, search for alternative solutions began. Spintronics, the shorthand form for spin based electronics is an example of a new technology. In spintronics, in addition to the fundamental charge of an electron, the intrinsic angular momentum of the electron and the associated magnetic moment can be used for memory applications.

The first implementation of this spintronics was shown in the giant magneto-resistance (GMR)[1] devices in multilayered metallic structures for which A. Fert and P. Grunberg were awarded the 2007 Nobel prize in physics[2]. In these devices the interaction of spins with magnetic materials was used for memory storage. Also another application of it was shown in the development of non-volatile magnetic random access memory MRAM[3].The very central theme in Spintronics is to have active manipulation of a single (ensemble) of spins in solid state devices, where **generation, manipulation** and **detection** of spins is possible in a controlled manner. Here spin is referred either to the single electron spin detected by its magnetic moment or average spin of ensemble of electrons because of applied magnetic field. In this thesis, the convention is that, up/down spin of an electron refers to majority/minority spin population parallel/antiparallel to the magnetization of the ferromagnet.

To answer this questions, one needs to inject a non-equilibrium spin population (spin polarization) in a system under consideration, usually in a non-magnetic material, and then study for how long the system can remember it's spin polarization and also be able to detect the non-equilibrium spins at a later time far away from the generation point. There are various experimental techniques to generate spin accumulation both at nano and macro-scales. Few examples include electrical spin injection[4], optical spin injection[5], spin pumping[6] and spin-orbit driven effects such as spin hall effect[7]. In this thesis we focus on the electrical spin injection from a ferromagnet to a nonmagnetic material. Ferromagnetic materials (FM), with unequal amount of majority (spin-up) and minority (spin-down) electrons at the Fermi energy, are used as spin injectors and detectors. Consequently, a charge current flowing in the bulk of the ferromagnet is spin polarized that, when in contact with a nonmagnetic material, induces a spin accumulation at the interface. The spin transporting channel (a semiconductor (SC) or a non-magnetic metal (NM)) is one of the main ingredients in spintronics devices. A Lot of research is devoted to find the best possible channel material which can transport spin over a long distance and time without losing spin information. Another research direction is to optimize the **injection**/**detection** of non-equilibrium spin population. In this thesis, the spin dependent properties of a NM material will be studied in a 3-terminal local device geometry. Thesis will discuss the concept of electrical spin injection and the modulation of spin accumulation with an applied external magnetic field. Analysis of the observed experimental results was done using the one dimensional standard theory of spin transport[8]. Furthermore a three-dimensional analysis using COMSOL mutliphysics was performed to corroborate the observation. The possible explanations for the universally observed disagreement between theoretical and experimental results is given.

### 1.1 Concept of spin injection and relaxation:

The density of states (DOS) for a FM and NM is shown in Fig. 1.1(a). At equilibrium, the DOS for spin up and spin down electrons is different for FM. On the other hand, the DOS for both spin species in NM is the same. When a current is sent through FM to NM interface, the spin imbalance of FM is created at NM, resulting in a net spin density (accumulation) at the FM/NM interface. This non-equilibrium spin accumulation in NM diffuses into the bulk of the NM and decays exponentially over a characteristic length scale called the spin relaxation length. Far away from the FM-NM interface, this net spin accumulation equilibrates (relaxes) via spin flip processes reaching the equilibrium (zero spin accumulation) condition.

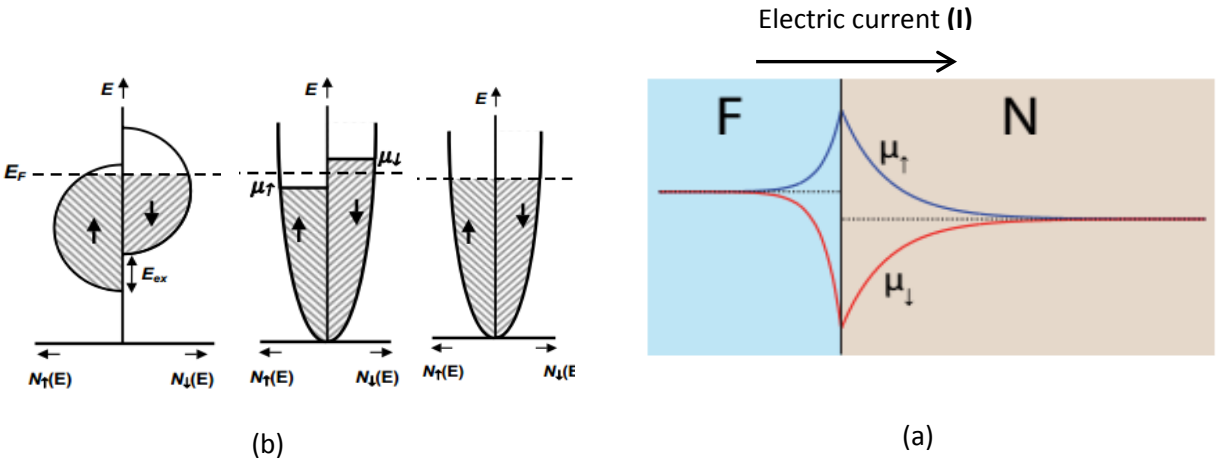


Figure 1.1: Adapted from reference [9] a) Energy band diagram showing the different DOS at Fermi level for spin up and spin down electrons. At the extreme right, energy band diagram for NM is shown at equilibrium condition. When current is sent through FM to NM, the spin population density for NM changes to its non-equilibrium condition showing net spin density. b) Spin accumulation profile for a FM-NM interface subjected to an electrical current. At the interface of both one sees the net spin accumulation which goes to equilibrium in bulk of the material.

In order to have an efficient spin injection, it is required that injected spins do not diffuse back in to the FM. Since the resistivities of FM and NM are comparable, and resistivity of SC is higher than FM, most of the injected spin will tend to diffuse back to FM[10]. This is known as a conductivity mismatch problem. To avoid this, a high resistive barrier (thin metal oxide layer) is created between FM and NM interface[11]. This high resistive barrier provides a large spin-dependent resistance which increases the spin polarization of the current. Also, a high resistive barrier at the detector electrode acts as an ideal voltage probe which makes spin detection efficient.

The studies of spin injection, spin transport and detection can be done in either in a non-local or local geometry. The non-local geometry for spin transport is widely used because it allows to separate pure spin current effects from any spurious charge current related effects to be interpreted as a spin signal[12]. But at the same time, the spin diffusion length of many non-magnetic materials is in sub-micron range, the spin injector and detector are separated by sub-micron length which requires nano-fabrication[13,14]. In a local geometry for spin transport, same ferromagnetic electrode is used as an injector and a detector and does not require any nano-fabrication.

### 1.2 Non-local 4 terminal geometry:

In a Non-local geometry, path of spin current through the channel is separated from the charge current such that one is able to create pure diffusive spin current. In this geometry at least two ferromagnetic (FM) electrodes are required, one for injection and another for detection. As shown in Fig. 1. 2 (a), a charge current is sent through one of the FM electrodes to the left side of the NM. This results in the accumulation of spins underneath the injecting FM contact that can be detected by the second FM. When the magnetization of both FMs are aligned parallel to each other, the measured 'non-local' resistance is lower compared to the case when these FM electrodes have anti-parallel magnetization. The width of these two FM electrodes is different which changes the coercive field of the FM electrode. Because of this, each FM electrode switches it's magnetization at different applied magnetic field. The typically observed change in the non-local resistance is shown in figure 1.2b. By varying the distance between the two FMs, spin transport properties of the channel, such as the spin relaxation length, can be obtained.

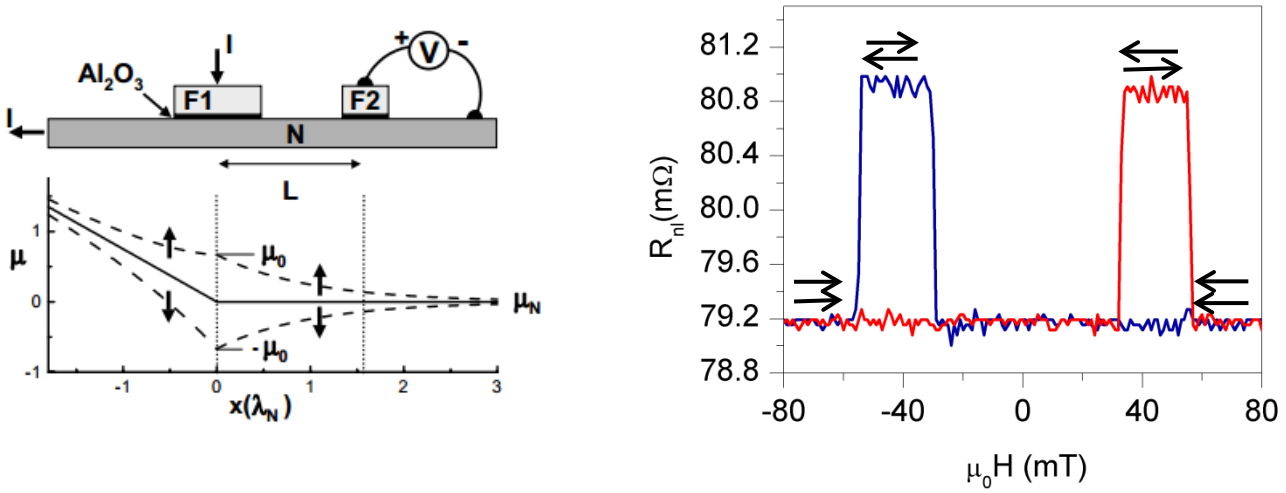


(a) (b)

Figure1.2: a) Schematic of non-local device geometry with two FM electrodes for spin injection and detection. FM electrodes are separated from NM channel by $Al_2O_3$ tunnel barrier[9]. The splitting of spin chemical potential is shown. The spatial dependence of the spin-up and spin-down electrochemical potentials (dashed) in the Al strip. The solid lines indicate the electrochemical potential (voltage) of the electrons in the absence of spin injection. b) The typical spin valve signal from non-local geometry showing selective switching of magnetizations of FM with a magnetic field. The small arrows represents the orientation of the magnetization of both FM. The red line represents the trace and blue one shows the retrace.

Another method to study the spin transport properties of devices, such as spin life time and spin diffusion length, is Hanle measurement. Compared to spin valve measurement, this technique has an advantage that the spin transport parameters of a given channel can in principle be extracted from a single device. In this type of measurements an external magnetic field is applied in a transverse direction to the injected spin direction. Because of the externally applied magnetic field, injected spins precess while travelling through the channel. The Bloch equation is used to describe the spin dynamics:

$$\frac{d\boldsymbol{\mu_s}}{dt} = D\nabla^2\boldsymbol{\mu_s} - \frac{\boldsymbol{\mu_s}}{\tau} + \boldsymbol{\omega_L} \times \boldsymbol{\mu_s}\,. \qquad (1.1)$$

The first term on the right hand side describes spin diffusion, the second term describes the spin relaxation and the last term explains the precession of spin with Larmor frequency. Here, D is the spin diffusion coefficient, τ is the spin relaxation time and $\boldsymbol{\omega_L} = \frac{g\mu_B}{\hbar}\boldsymbol{B}$ , being Larmor frequency with $\boldsymbol{B}$ as the external magnetic field. Bold letters represent the vector. The spin chemical potential $\boldsymbol{\mu_s}$ is a 3-dimensional spin accumulation needed to describe the spin dynamics of a Hanle measurement. In a steady state system with $\frac{d\boldsymbol{\mu_s}}{dx}$ = 0 and $\mu_s(\infty) = 0$, $\mu_s$ decays exponentially as$\exp(-x/\lambda)$ . Where λ = $\sqrt{D\tau}$ is the spin relaxation length of a non-magnetic channel.

**1.3 Local 3-terminal geometry:**

As the name implies, the local three terminal measurement probes the spin accumulation locally. In this technique the spin accumulation is probed just underneath the FM electrode which is injecting the spins. When compared to non-local geometry, in local geometry same FM electrode is used to **inject** and **detect** the spin accumulation under the ferromagnetic contact, meaning the path of spin current is same as the path of charge current. Furthermore the interface is biased and that results in a lower signal to noise ratio for the local spin current detection and it also activates inelastic processes, when the tunnel barrier contains impurities. Nevertheless, this geometry allows to choose arbitrary junction area which helps in improving signal to noise ratio. A typical 3-terminal local geometry device is as shown in figure 1.3 showing a tunnel barrier, usually MgO or $Al_2O_3$, sandwiched between a FM and NM. In order to have uniform spin accumulation in the spin accumulation volume, the device dimensions have to satisfy the condition $W_F, W_N \ll \lambda_N \ll d$, where $W_F$ is the width of FM contact, $W_N$ is the width of NM contact, $\lambda_N$ is spin diffusion length of NM and d is the device dimension in z-direction. In this case, diffusion of spin accumulation out of the injection volume can be disregarded.

The detection of spin signal is done by Hanle measurements as mentioned earlier. A detailed explanation of the technique can be found in chapter 2 of this thesis. The spin dynamics is studied with Bloch equation without the diffusion term:

$$\frac{d\boldsymbol{\mu_s}}{dt} = -\frac{\boldsymbol{\mu_s}}{\tau} + \boldsymbol{\omega_L} \times \boldsymbol{\mu}_S \,. \qquad (1.2)$$

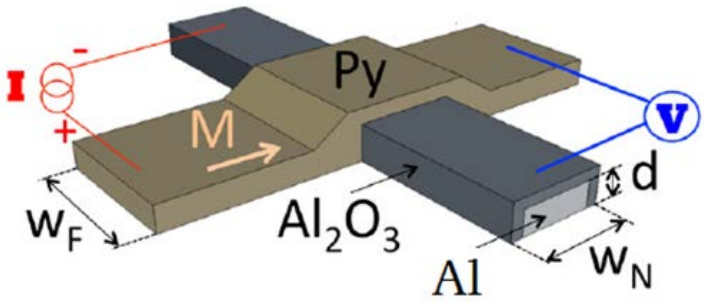


Figure 1.3: Adapted from reference[15]. Typical local 3-terminal device geometry for spintronics devices showing an AlOx tunnel barrier separating Permalloy and Aluminium.. The magnetization of FM(Py in this case) is along it's easy axis. For Hanle measurements the external magnetic field is applied perpendicular to
magnetization of FM.

While this technique is simple to implement and is widely used in the study of spin injection in various semiconducting materials and metals, numerous open questions remain and the experimentally observed results are controversial because of following reasons;

1. The total spin signal measured with this geometry cannot be explained using a standard theory for spin injection and accumulation. The measured signals are 8 orders of magnitude higher than expected from one dimensional standard theory. In this thesis a three dimensional spin transport model implemented in COMSOL multiphysics 4.3 also yields very small spin accumulation signals that are hardly visible in experiments.
2. The bias and temperature dependence of the measured spin signal does not agree well with tunneling spin polarization[15]. Specifically, the signal is usually larger in one biasing direction and is often absent in the reverse biasing condition. Although initial studies focused in explaining this asymmetry based on differences in energy dependence of the spin polarization, recent studies provide alternative explanation based on impurity driven mechanism (Pauli spin blockade)[16] that are only energetically favored in one biasing condition than the other. Alternative explanation was put forward by Appelbaum et al[17]. where the role of the impurities is identified using inelastic electron tunneling spectroscopy.
3. The spin life time extracted from these measurements is always two orders of magnitude lower than those values measured by Electron spin resonance experiments[18,19]. Also it does not vary much with respect to type of carrier in the semiconductor, doping level or temperature and type of semiconductor[20]. The spin life time is also invariant for different metals with significantly different spin-orbit coupling[15].
4. It is also shown that the Hanle signals are observed in 3-terminal devices with NM/I/NM layers[16]. This suggests that the observed Hanle signals are not just the property of spin injection as in these devices there is no FM to inject spins.

Recently it was also shown theoretically that when an electric current is passed from a FM into a NM, spin dependent temperature can also be induced via the spin polarization of the Peltier coefficient[21]. This non-equilibrium temperature difference between the spin-up and the spin-down electrons can also result in a non-negligible thermo-voltage signal that also adds up on the regular electrical induced non-equilibrium spin accumulation induced voltage. This process only explains the variation in the spin life times extracted from width of measured Hanle signal. This is because of the fact that the spin heat accumulation created by the spin dependent temperature has a line width set by the spin heat relaxation time, which is estimated to be $1/5^{th}$ of the electrical spin relaxation time. The effective spin life time is therefore determined by the smallest of the two and effectively broadening and varying the line widths of total Hanle signal.

Furthermore, one of the possible origins of the measured signals in this configuration can be attributed to inelastic tunneling through junction. Since the detector junction in 3-terminal geometry is biased and tunneling current flows through, it is possible that contributions from inelastic tunneling due to impurities in the tunnel barrier can be significant. To study such contributions, inelastic tunneling spectroscopy (IETS) techniques can be used[17]. The secondary tunneling because of specific resonances increases the total conductance of the junction. These resonance processes are activated because of the electrostatic potential energy provided by voltage biasing to the detector junction. The increased conductance of the barrier can be seen by thermally broadened peak in the second derivative of I-V curve, which can be measured by second harmonic response with a lock-in amplifier.

This thesis will present research done in 3-terminal spintronics devices to understand the physics behind it in a better way. The second chapter of the thesis introduces the basic of spin transport and the physics of different aspects of 3-terminal spintronics devices. Next chapter discusses the experimental techniques employed for fabrication of 3-terminal spintronics devices. Chapter four presents the analysis of the measurements and discusses the possible physics for different measurements.

# Chapter 2: Theoretical Background

**2.1 The two channel model:**

Spin transport in a diffusive metal can be understood with the help of the two channel model, one for spin-up and another for spin-down electrons. First proposed by Valet and Fert[8], this theory has proved to be important in explaining various spintronic and spin caloritronic phenomena in nonlocal and pillar spin valve structures. In general the conductivity of a material is defined by Einstein relation

$$\sigma = De^2N(E_F)\,. \tag{2.1}$$

Here D is the diffusion coefficient, e is the electron charge and $N(E_F)$ is DOS of electron at Fermi energy $E_F$. The DOS in FM is different for spin up (↑)and spin down (↓)electrons which results in different conductivities $\sigma_\uparrow$nd $\sigma_\downarrow$respectively. The total conductivity is given by

$$\sigma = \sigma_\uparrow + \sigma_\downarrow\,, \tag{2.2}$$

Also the diffusion coefficient is spin dependent and spin dependence of conductivities is determined by both DOS and spin dependent diffusion coefficient.

$$D_\uparrow = \frac{1}{3}v_{F\uparrow}l_{e\uparrow} \text{ and } D_\downarrow = \frac{1}{3}v_{F\downarrow}l_{e\downarrow}. \tag{2.3}$$

Because of spin dependent conductivities, the current flowing through the FM is spin-polarized and is given by

$$j_\uparrow = \frac{\sigma_\uparrow}{e}\frac{\partial\mu_\uparrow}{\partial x} \text{ and } j_\downarrow = \frac{\sigma_\downarrow}{e}\frac{\partial\mu_\downarrow}{\partial x}\,, \tag{2.4}$$

with the current polarization in the bulk of FM :

$$\alpha = \frac{\sigma_\uparrow - \sigma_\downarrow}{\sigma_\uparrow + \sigma_\downarrow}\,. \tag{2.5}$$

By considering spin flip processes (the flipping of spin up into spin down and vice versa) and the conservation of particles, one obtains the following equation:

$$\frac{1}{e}\nabla.j_\uparrow = -\frac{n_\uparrow}{\tau_{\uparrow\downarrow}} + \frac{n_\downarrow}{\tau_{\downarrow\uparrow}}\,, \tag{2.6a}$$

$$\frac{1}{e}\nabla.j_\downarrow = -\frac{n_\downarrow}{\tau_{\downarrow\uparrow}} + \frac{n_\uparrow}{\tau_{\uparrow\downarrow}}\,, \tag{2.6b}$$

with

$$\frac{N_\uparrow}{\tau_{\uparrow\downarrow}} = \frac{N_\downarrow}{\tau_{\downarrow\uparrow}}\,. \tag{2.6c}$$

So that there is no spin scattering in the equilibrium condition. Generally spin flip times are larger than momentum scattering time $\tau_e = l_e/v_F$, because of which the transport can be explained using the diffusion of two spin species. Combining equations 2.4, 2.5, 2.6 and 2.1; one obtains

$$D\frac{\partial^2\mu_\uparrow-\mu_\downarrow}{\partial x^2} = \frac{\mu_\uparrow-\mu_\downarrow}{\tau}, \tag{2.7}$$

where τ is the time scale over which non-equilibrium spin accumulation $(\mu_\uparrow - \mu_\downarrow)$ decays.

Applying this formulation to the three-terminal device geometry one can study the spin dependent properties of the material under study.

**2.2 Finite element modelling:**

To fully understand the relevant thermal and electrical properties we employ the three dimensional finite element model developed by Slachter *et al*[22] to our 3-terminal device geometry. To model spin dependent transport, the software package Comsol Multipysics is used. A set of Partial Differential Equations (PDEs) are used to study spin transport. The spin dependent currents $J = (J_\uparrow, J_\downarrow)^T$, are defined as:

$$\boldsymbol{J} = -\boldsymbol{c}\nabla\boldsymbol{u}, \tag{2.8}$$

here $\boldsymbol{u} = (\boldsymbol{V}_\uparrow, \boldsymbol{V}_\downarrow)$ is spin dependent voltages and, the spin dependent conductance matrix $\boldsymbol{c}$ defined as (for an isotropic case);

$$\boldsymbol{c} = \begin{pmatrix} \sigma_\uparrow & 0 \\ 0 & \sigma_\downarrow \end{pmatrix}. \tag{2.9}$$

The conservation of charge and spin currents are given by following equations:

$$\boldsymbol{\nabla}.(\boldsymbol{J}_\uparrow + \boldsymbol{J}_\downarrow) = 0, \tag{2.10}$$

$$\nabla \cdot J_s = \nabla^2(V_\uparrow - V_\downarrow) = \frac{V_\uparrow - V_\downarrow}{\lambda^2}, \tag{2.11}$$

here $\lambda = \sqrt{D\tau}$ is the spin relaxation length. The PDEs for bulk materials are determined by conservation of fluxes:

$$\boldsymbol{\nabla}.\boldsymbol{J} = \boldsymbol{f}(\boldsymbol{u}), \tag{2.12}$$

where $\boldsymbol{f}(\boldsymbol{u})$ is the source term. Considering a spin polarization as:

$$P = \frac{(\sigma_\uparrow-\sigma_\downarrow)}{(\sigma_\uparrow+\sigma_\downarrow)}, \tag{2.12}$$

the source term is given by:

$$f = \frac{(1-P^2)}{4\lambda^2}\sigma(V_\uparrow - V_\downarrow).\begin{pmatrix}-1\\1\end{pmatrix} \quad (2.13)$$

This model was applied to the 3-terminal devices which includes the tunnel barrier as a very high resistivity FM with a bulk spin polarization equal to the tunnel spin polarization. The spin voltages are calculated for varying polarization of FM electrode and tunnel barrier. Also the thickness of a NM and a FM are varied. Calculated spin accumulation is then compared with the 1-dimensional modelling results reported[15].

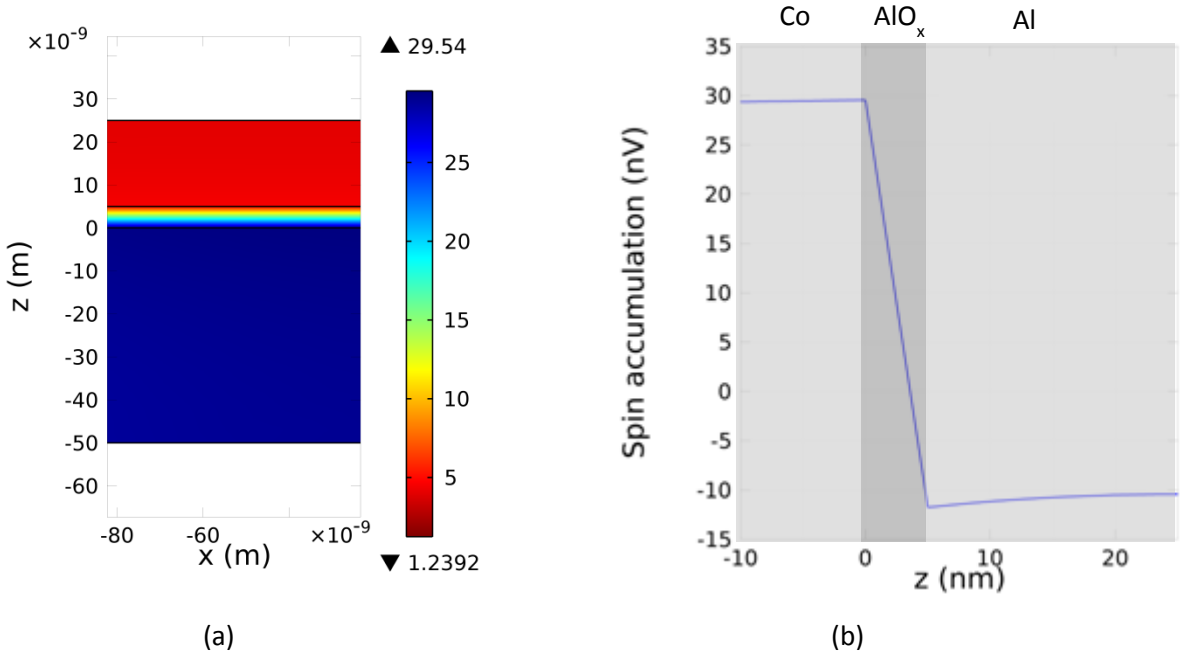


Figure 2.1: Figure shows the results of finite element modeling for 3-terminal local geometry devices. The Al layer has a thickness of 50 nm, Co of 25nm and $AlO_x$ barrier of 5 nm thickness. A 10 $\mu$A current is passed from Co to Al and calculated spin accumulation is plotted. a) shows the total spin accumulation underneath the junction area in Al as well as in Co layer in Z-X plane. The magnitude of spin accumulation is highest and it is 29.54 nV. b) shows the line plot of spin accumulation in Z direction. Spin accumulation in Al decays with spin relaxation length of 350 nm and it also decays in Co but very slowly as spin relaxation length of 40 nm is taken for this calculations.

**2.3 Simmons model:**

One of the most important aspects in spintronics devices is tunneling through insulating barrier. The process of tunneling through metal-insulator-metal junctions was first put forward by Frenkel, Sommerfeld and Bethe[23]. Simmons solved the tunneling problem for a simple rectangular model within WKB approximation and provided the current density relationship with the applied bias for various regimes of the tunnel process.

Consider the potential schematic of tunnel barrier as shown in figure 2.2. Two metals are separated by a thin insulating barrier of width t and barrier height $\varphi$. A voltage bias is applied across the barrier such that the Fermi levels of both the metals are shifted with respect to each other. In the process of tunneling, the electron has to tunnel from an occupied state in one metal to an unoccupied state in other one. The tunneling current density is given by,

$$j \propto \int_{-\infty}^{+\infty} N_1(E)N_2(E-eV)D(E)f(E)dE \qquad (2.14)$$

where $N_1(E), N_2(E-eV)$ is the DOS for metals, $D(E)$ is the probability of an electron to tunnel through the barrier and $f(E)$ is the Fermi distribution function of the electrodes.

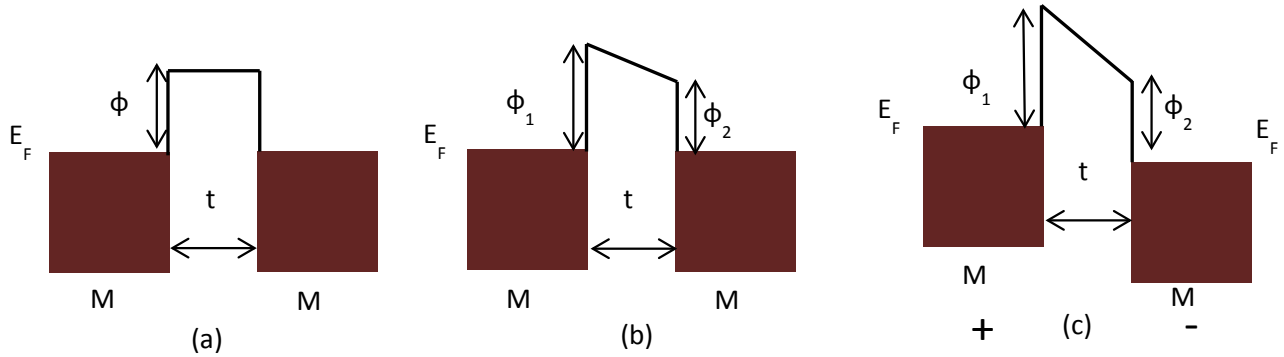


Fig 2.2: a) Simple rectangular potential barrier considered by Simmons. $\varphi$ is the barrier height in $eV$ and t is the barrier thickness in Å. b) The tunnel junction as in Brinkmann's model with modification to Simmons model to include asymmetry in the work function of the electrodes giving rise to a trapezoidal potential barrier. c) shows the shifting of Fermi levels of two metals because of applied bias.

The net tunneling current is given by the difference in currents flowing in opposite direction through the junction,

$$j = j_{1\to 2} - j_{2\to 1}\ ,$$

$$j = \frac{4\Pi}{\hbar}\int_{-\infty}^{+\infty} N_1(E)N_2(E-eV)D(E)\big(f(E)-f(E-eV)\big)\,dE\ . \qquad (2.12)$$

The simplest case of rectangular tunnel barrier exist when both the metals have the same Fermi energy level and identical interfaces with an insulating barrier. For the biasing of eV < $\varphi$, the net current will be given by,

$$j = \frac{e}{\hbar(2\Pi t)^2} \times \left[\left(\varphi - \frac{eV}{2}\right) exp\left(-\alpha t\sqrt{\varphi - \frac{eV}{2}}\right) - \left(\varphi + \frac{eV}{2}\right) exp\left(-\alpha t\sqrt{\varphi + \frac{eV}{2}}\right)\right], \quad (2.13)$$

with α = $2\sqrt{2m}/\hbar = 1.025/(\text{Å}\sqrt{eV})$, where m is electron mass and ħ is reduced plank's constant.

Expanding this equation for eV≪ $\varphi$, up to the third power and replacing the natural constants by their numerical values gives:

$$j = 3.16 \times 10^{10} \frac{\sqrt{\varphi}}{t} exp\left(-1.025t\sqrt{\varphi}\right)\left(V + \left(0.0109\frac{t^2}{\varphi} - 0.032\frac{t}{\varphi^{3/2}}\right)V^3\right). \quad (2.14)$$

By using Eq. (2.14), the barrier height and the thickness of the barrier can be obtained. In reality, the metal electrodes have different interface properties which change the case of simple rectangular barrier. This difference can, for example, arise from the difference in the work function of the metals used. Brinkman accounted for this asymmetry and used the trapezoidal barrier as shown in figure 2.2b. With a potential $\varphi(x) = \varphi_1 + \frac{x}{t}(\varphi_2 - eV - \varphi_1)$, Brinkman model gives the accuracy of ~10% for barriers thicker than 1 nm and for $\Delta\varphi/\overline{\varphi} < 1$:

$$j = 3.16 \times 10^{10} \frac{\sqrt{\overline{\varphi}}}{t} exp\left(-1.025t\sqrt{\overline{\varphi}}\right)\left(V - 0.0213\frac{t\Delta\varphi}{\overline{\varphi}^{3/2}}V^2 + 0..0109\frac{t^2}{\overline{\varphi}}V^3\right). \quad (2.15)$$

With j being current density in Å/cm$^2$.

If the I-V curves shows a weak temperature dependence, it suggests that the dominant process behind the tunneling is a direct elastic tunneling. The direct tunneling of an electron directly from a FM electrode to a NM electrode is pronounced when there are no or little localized states inside the tunnel barrier. In such a barrier, the conductivity depends on the tunnel barrier thickness as shown below[24]:

$$G^{dir} = G.\exp(-2\alpha t), \quad (2.16)$$

With $\alpha^{-1}$ as the localization length. The direct tunneling is dominant when $t$ and $\alpha^{-1}$ are comparable. The conductivity in direct tunneling depends on the temperature weakly because of the thermal broadening of the Fermi function of electrodes[24]:

$$I(T) = I(0)\frac{CT}{\sin CT},$$

with C= 1.384x10$^{-4}$ $(t/\sqrt{\varphi})$ and $T$ is temperature.

For higher number of impurity states, the inelastic tunneling process dominates over the resonant and direct tunneling. In this process, the tunneling from electrode to impurity states and from impurity states to other electrode is elastic but hopping between two impurity states is inelastic in nature. Glazman and Matveev had shown that the conductivity for the inelastic tunneling is:

$$G_2^{hop} \propto T^{4/3}.\exp\left(-\frac{2\alpha t}{3}\right), \tag{2.17}$$

for N number of defects in the tunnel barrier and for small voltages $eV \ll k_B T$. For the case of large number of localized states, the lower bias limit conductivity can be generalized as:

$$G_N^{hop} \propto T^{N-(2/(N+1))}.\exp(-2\alpha\, t/(N+1)) . \tag{2.18}$$

In our analysis, we use the Brinkman model to characterize the tunnel barrier used for our 3-terminal devices and estimate the values of barrier height and barrier thickness.

**2.4 Hanle effect and impact of interface roughness and in-plane external magnetic field on it:**

The Hanle effect is a standard test for spin injection in NM materials. It refers to the process in which ensemble of oriented spins diphase in an external magnetic field ($B_{ext}$) due to the Larmor precession. When an external magnetic field, much smaller than the out of plane anisotropy field of the FM, is applied in a transverse direction to injected spins, the spins preces around this applied field. As a result, the projection of the total spin accumulation parallel to the magnetization of FM is reduced. This decrease in the spin accumulation is a function of $B_{ext}$ with Lorentzian line shape;

$$\Delta\mu(B_{ext}) = \frac{\Delta\mu(0)}{1+(\omega_l\tau)^2}. \tag{2.19}$$

The FWHM of Lorentzian line shape gives the spin-life time $\tau$. Figure 2.3 shows the schematic of typical Hanle curve for 3-terminal devices.

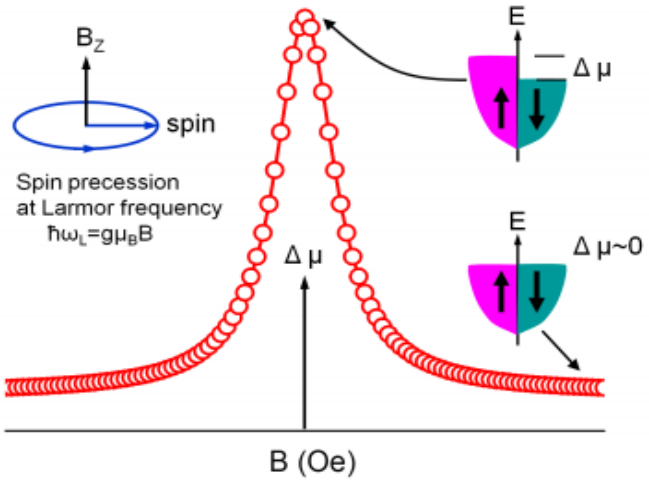


Fig 2.3: Figure shows the typical Hanle signal observed in external magnetic field[25]. Inset shows the direction of external magnetic field and the direction of ensemble of accumulated spins. At zero external magnetic field the spin accumulation is highest and as magnetic field strength increases the injected spins starts precessing about the direction of magnetic field which causes the decrease in spin accumulation. At high enough magnetic field spin accumulation goes to zero.

The deviations from Lorentzian line shape have been observed and possible explanation for this deviation were put forward[25,26]. In reality, the FM-insulating barrier-NM interfaces are not uniform. The electrons are injected from FM to NM with spins parallel to the interface. Because of the finite roughness of the interface, strong local magneto-static fields are present that affect the spins injected in NM. Sharma *et al* treated these magneto-static fields as a sinusoidal variation with period λ, as shown in figure 2.4.

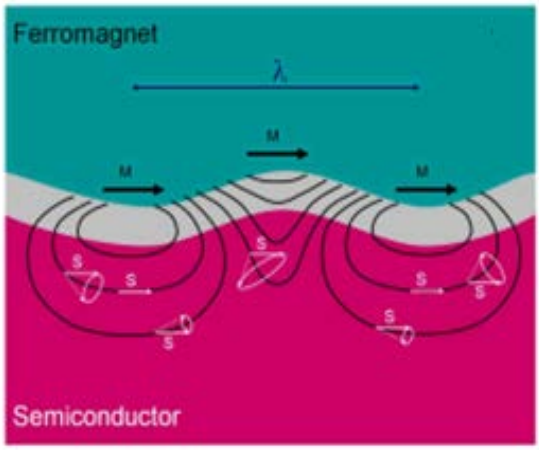


Figure2.4)The sinusoidal interface roughness causes the precession of injected spins on different trajectories as shown here[27].

The magnitude and direction of these magneto-static fields are inhomogeneous and change periodically. The strength of these fields, linearly related to the type of FM and its saturation magnetization, decreases exponentially from the interface. The decay length is determined by the period of interface roughness λ. The black lines in figure 2.4 shows the magnetic field lines because of local magneto-static fields. In the local magneto-static fields, the spins precess on different trajectories as shown in the figure by dotted arrows. In the presence of this roughness, a spin accumulation is reduced because of the spin precession from magneto-static fields. This reduction in spin accumulation is strongest at the interface which is the place where spin detection takes place. Also it has been observed that when different FM materials are used, the width of Lorentzian line shape changes. This suggests that the broadening of Lorentzian line shape is not solely defined by the properties of transport channel as described by equation(2.16), but also depends on the type of FM used . This effect was investigated for various FM metals such as Co, Fe, Ni in the order of decreasing saturation magnetization value that directly determine the local magneto-static fields. This phenomenon is referred as Inverted Hanle effect. In this case, the spin accumulation increases with increasing lateral magnetic field. At smaller lateral magnetic field, the local magneto-static fields are strong enough to reduce the total spin accumulation. But when large enough magnetic field is applied in-plane, this forces local magnetic fields to align themselves with externally applied in-plane field and hence one observes increase in spin accumulation. Therefore in general, the extracted spin-life time should be taken as a lower limit on actual spin-life time.

Also if externally applied magnetic field is not perfectly perpendicular to the spin direction of injected electrons because of experimental setup, then this will lead to angle dependent Hanle signals. One can get a quantitative understanding of angular dependence of externally applied transverse magnetic field on spin accumulation. Consider magnetic field being applied in XZ plane with orientation ranging from into the plane to out of the plane. Starting with Bloch equation for 3-terminal devices as shown in equation (1.2), an analytical solution under any applied magnetic field can be obtained as follows:

$$\mu_{sx} = \mu_0 \left( \frac{\omega_x^2}{\omega_{tot}^2} + \frac{\omega_y^2+\omega_z^2}{\omega_{tot}^2} \frac{1}{1+(\omega_{tot}\tau)^2} \right). \quad (2.20)$$

To include the effect of local magneto-static fields $B_i^{ms}$ caused by interface roughness, the total magnetic field $B_i^{ext}$ is taken as

$$B_i = B_i^{ext} + B_i^{ms}, \quad (2.21)$$

with $(i = x, y, z)$, which includes the contributions from external and magneto-static fields. If the magneto-static field has a spatial variation with period λ then it is written as:

$$B_i^{ms}(x) = B_i^{ms}(0).\cos(2\Pi x/\lambda). \quad (2.22)$$

If spin diffusion length is much larger than λ, the total average magnetic field is taken as:

$$\boldsymbol{B}_i^2 = \left(B_i^{ext}\right)^2 + (\boldsymbol{B}_i^{ms})^2 \quad (2.23)$$

And equation (2.20) becomes,

$$\mu_{sx} = \mu_0 \left( \frac{(\boldsymbol{B}_x^{ms})^2+\left(B_x^{ext}\right)^2}{B_{tot}^2} + \frac{(\boldsymbol{B}_\perp^{ms})^2+\left(B_z^{ext}\right)^2}{B_{tot}^2} \frac{1}{1+(g\mu_B/\hbar)^2(B_{tot}\tau)^2} \right) \quad (2.22)$$

where $\overline{B}_x^{ms}$ and $\overline{B}_\perp^{ms}$ represent average magneto-static field parallel and perpendicular to the injected spins, respectively. Figure 2.5 shows the simulation of the above equation with assumed parameters $\tau$= 0.9 ns, $\overline{B}_x^{ms}$ = 0.270 G and $\overline{B}_\perp^{ms}$ = 440 G.

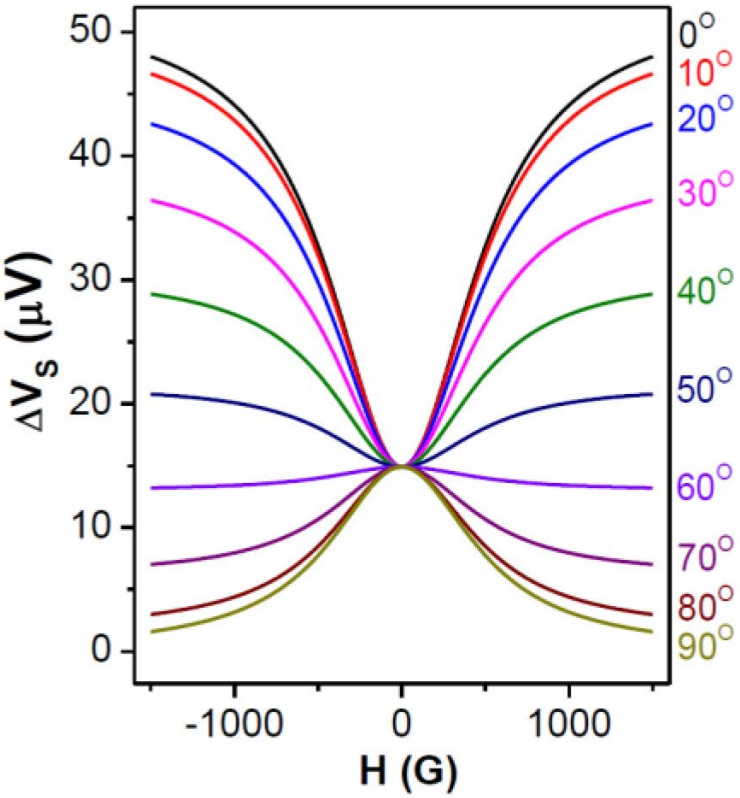


Figure 2.5: Adapted from reference[26]. Figure shows the simulated curves for spin signal modulation with respect to perpendicular external magnetic field. As the angle between the spin orientation of injected electrons and the external field changes from 90 to 0 , the modulation of spin accumulation changes. At nearly 60 angle between two, the Hanle signal changes its sign and gives the inverted Hanle type results.

# Chapter 3 : Experimental Section

In the fabrication process of 3-terminal devices, first the bottom layer of a NM metal (Al) is created. This NM metal layer is then exposed to $O_2$ to form an oxide layer ($AlO_x$) either by plasma oxidation or natural oxidation. After the formation of the oxide layer, a FM layer (Py or Co) is deposited in cross geometry as shown in figure 3.3. A contact electrode layer of Au is deposited on top of FM layer. In our study, two types of devices were prepared. Type A consists of long bars of FM and Type B had a ferromagnet only patterned on top of the Al bar. All the measurements that will be discussed in this thesis are from TYPE B only.

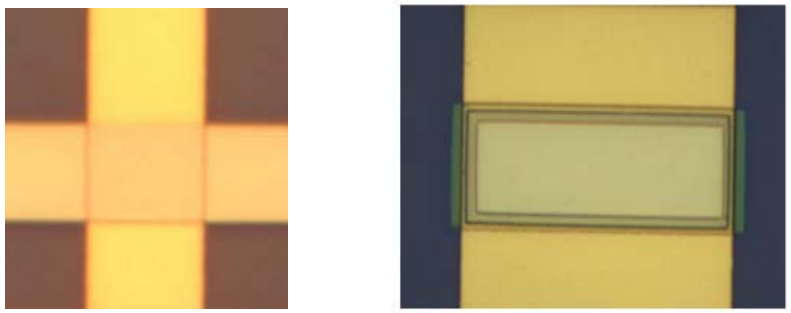

(a) (b)

Figure 3.1: Figure shows the two different types of devices fabricated. a) shows the type A devices with a long bar of a FM. b) shows the B type of device with FM being deposited only on the Al bar.

**3.1 Fabrication details:**

The 3 terminal devices were fabricated using standard lithography techniques. The devices are patterned on a micrometer or nanometer scale using optical or e-beam lithography, respectively. For the former we used a light sensitive resist whereas for the latter a poly methyl metacrylate (PMMA) based e-beam sensitive resist was used. In the case of an e-beam sensitive resist the focused electron beam is used to expose the resist and in case of a light sensitive resist an ultra-violet light source is used. In the technique of lithography, the substrate is exposed with the help of a mask with a desired pattern. The standard steps in lithography techniques are shown in a figure 3.2.

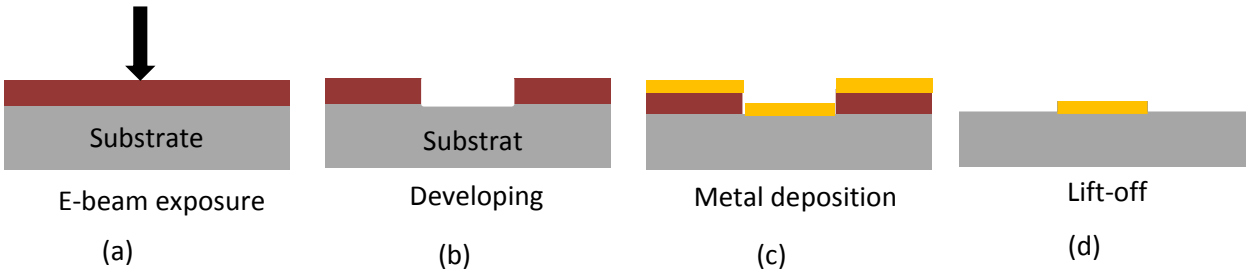


Figure 3.2: Different lithography steps. a) shows the e-beam exposure to write the desired pattern on the substrate. b) Shows the substrate after development. The part of polymer which is exposed by e-beam gets dissolved in development process. c) shows the deposition step in which desire material is deposited on whole substrate. d) shows the substrate after lift-off process. The material

After the exposure, the exposed part of resist is removed by the process of development using a solvent. In this case the used resist is called a positive photoresist. In a negative photoresist, the unexposed part is removed from the substrate by the solvent. The substrate which is covered with remaining resist can be used for depositing required materials. In the last step of lithography, the remaining resist is removed thus lifting off the deposited materials on top of the resist.

To efficiently inject spins and also to avoid conductivity mismatch problems, tunnel junctions are inserted at the interface of FM and NM. We used two different processes to grow the tunnel barriers between the junction of a NM and a FM by either $O_2$ plasma oxidation, or natural oxidation. For plasma oxidation, a power of 60 watts was used at the pressure of $10^{-1}$ millitorr. To find optimum tunnel junction properties, different devices were fabricated using plasma oxidation for 15 sec, 30 sec, 45 sec and 60 sec. The second type of tunnel barriers were made using a natural oxidation process where it was shown recently that these types of barrier support large density of impurities in the tunnel. To that end, the natural oxidation was done in multiple steps. First a 0.6nm Al layer was deposited at a rate of 0.5nm/sec followed by 20 minutes oxidation at an oxygen pressure of $10^{-1}$ millitorr higher in some cases. The oxidation processes were done in the load-lock of the electron gun evaporator (temescal 2000) after depositing the Al layer. A sputtering system (Kurt J. Lesker) was also used for deposition for reasons stated later in this chapter. Oxidation in the sputtering system was also carried out in the load-lock. Performing oxidation in the load-lock of both the systems ensures that no harm is done to the high vacuum of deposition chamber of these systems.

**Photolithography :**

These 3 terminal devices do not involve any submicron sized features, therefore the photo lithography techniques were used. The involved steps are as follows;

**Resist coating**

A clean and dry $Si/SiO_2$ substrate is coated with 907/12 photoresist polymer at 4000 RPM for 60 seconds. After spin coating, the substrate is baked at 120 $^0$C for 60 seconds which creates a uniform thickness of 150 nm resist.

**Patterning**

Certain areas of the sample are exposed using an UV light source with the help of a mask. At the exposed regions, the resist decomposes in to a lower molecular weight polymer compared to the unexposed regions.

**Development**

After exposure the sample is put in OPD 4262 developer for 60 seconds followed by rinsing in deionized (DI) water for 5 minutes. The broken polymer gets dissolved in the developer and one gets the negative image of the removed polymer on the sample.

**Deposition**

Electron gun evaporation:

Thin layers of desired metals are deposited on top of the entire sample using e-beam evaporation. This deposition is done at rate of 0.1nm/sec inside a vacuum chamber at a base pressure of 2e-6 Torr. A target of the desired metals is evaporated by an electron beam and deposited on the sample until desired thickness is reached. During the electron gun deposition, there were issues with power stability for Al which resulted in a rough Al layer.

Sputtering:

In addition to electron gun evaporation, a sputtering system is also used to deposit the required material. Sputtering was used over electron gun evaporation because the surface roughness of deposited Al was high which in turn was detrimental the quality of the tunnel barrier. The surface roughness of the sputtered Al layer was better and at the same time the plasma oxidation process can be done in a more controlled manner compared to when electron gun evaporation is used. Since the deposition done by sputtering is isotropic, a better resist profile is needed as compared to electron gun deposition.

**Lift off**

The sample is then put in heated acetone (50 $^{0}$C) for more than 5 minutes, to remove the remaining polymer and the deposited metals on top of it. Only deposited layers at the developed part of the polymer stay on the substrate. The final device, shown in figure 3.2, presented a problem in that the OPD4263 developer attacked the Al metal layer. Because of this the junction areas were broken as shown below:

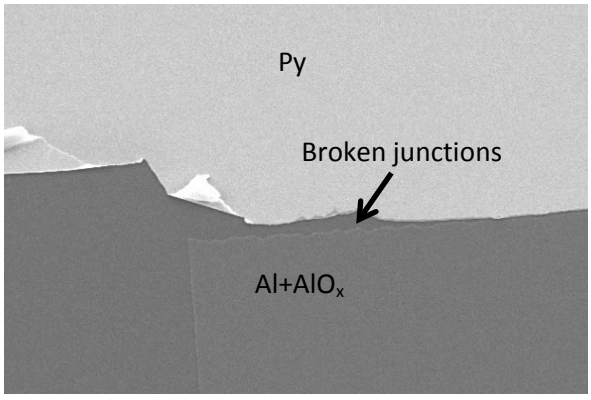


Figure 3.2: The junction area of the 3-terminal device fabricated using photolithography. The developer used for this process etches the Al layer, resulting in broken junctions.

**E-beam Lithography :**

**Resist coating**

A clean and dry $Si/SiO_2$ substrate is coated with a PMMA (971K 4%) polymer layer at 4000 RPM for 60 seconds. After spin coating, the substrate is baked at 180 $^0$C for 90 seconds which creates an even layer of 270 nm resist. For crosslinking (to be discussed later), PMMA 971K 3% polymer was used. This gives the thickness of a resist of 150 nm at 4000 RPM in 60 seconds.

**Patterning**

Certain areas of the sample are exposed using an e-beam source with the help of a polymer mask. The device structure is first designed using the e-LINE program; we used different layers for each components of the device. The EBL is done using a Raith 150 electron beam lithography system by selecting the layer of interest.

**Development**

After exposure, the sample is put in a mixture of a methyl isobutyl ketone (MIBK) and isopropyl alcohol (IPA) for 30 seconds. The mixture is made in 1:3 proportion by volume. After this, the sample is put in IPA for another 30 seconds to remove all the MIBK from the sample. The broken polymer gets dissolved in the developer and one gets the negative image of polymer on the sample.

**Deposition**

The deposition is done using both electron gun evaporation and sputtering as discussed earlier.

**Lift off**

The sample is then put in warm acetone (45 $^0$C) for more than 5 minutes, thus removing the remaining polymer and the deposited metals on top of it so that deposited layers only stays on the developed part of the sample.

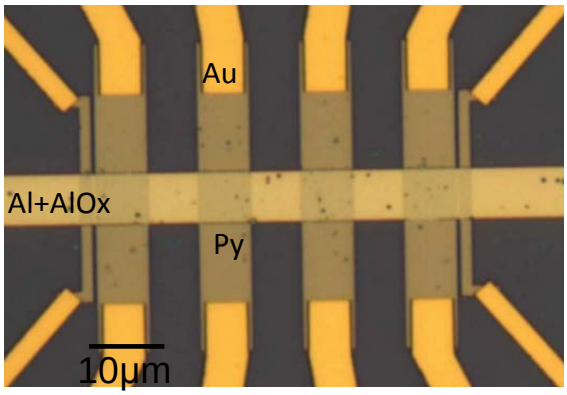


Figure 3.3: 3-terminal device fabricated during the thesis research. The device shows the FM of different width which enables to study the non-local spin valve type measurements. Also the edges at the interface of Py and Al were broken.

During the fabrication of devices, the FM layer was not uniformly covering the Al layer, resulting in broken edges. To overcome this problem, a pillar geometry was used to fabricate the devices. In the pillar based structures (shown in figure 3.4a) the deposition of the NM layer, the tunnel barrier and the ferromagnetic injector is done in-situ without breaking the vacuum of the deposition chamber. The top contact of Au is done after opening a contact-hole in another e-beam lithography step and making sure that an electrical short between the top electrode and FM layer is avoided using a cross linked polymer[28].

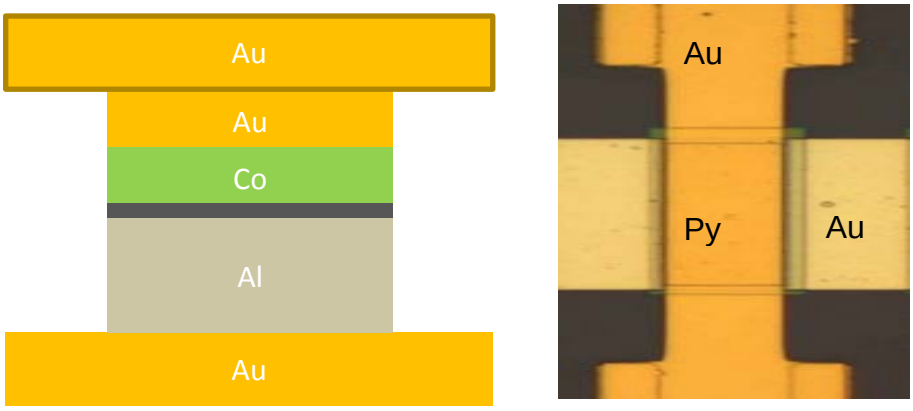


(a) (b)

Figure3.4:
a) Schematic of the 3-terminal pillar structure is shown. A Co/AlOx/Al pillar structure is sandwiched between top Au- and bottom Au-contacts.
b) Fabricated device of3-terminal pillar. Use of cross-linked polymer is done to have electrical insulation between contact electrode and FM layer.

### 3.2 Measurement setups and techniques:

#### Measurement setups

The fabricated samples are glued on a chip carrier using GE varnish and all contacts are connected to the chip carrier by wire bonding. The chip carrier is then mounted on a sample holder, which is placed between the poles of an electro-magnet. The sample is connected by a switch box with which one can selectively connect desired electrodes/junctions under measurements. IV measurements and some transport measurements are done using IV-measurement box and Lock-in amplifier controlled by Lab View. The Lock-in amplifier is able to supply a sinusoidal voltage and measures the voltage ($V_{in}$) returned from the sample via the IV-measurement box. The Lock-in frequency for the measurements was set around 17 Hz. The I-V-converter box sources the current which is controlled by output voltage ($V_{out}$) of a Lock-in amplifier. It also has a pre-amplifier which amplifies the voltage from the sample which is later fed to the input of the lock-in amplifier. The lock-in amplifier has the capability to significantly reduce the noise in measurements by multiplying the signal $V_{in}$ with a 90 degree phase shifted reference signal and integrating over the time constant (0.3 sec for -measurements). Because of this, the Lock-in is able to filter out all other frequencies present in the output hence reducing the noise. Also, for dc measurements and IV characterization; a Keithley 2410A source-meter which is capable of

simultaneously sourcing and measuring. Most of the measurements discussed in this thesis are performed using this DC measurement setup.

**Measurements**

Initially charge transport measurements are done to characterize the electrical contacts and junctions from the samples using the following measurement configurations;

**2-probe:**

For every newly fabricated sample 2-probe measurements are done to check if all the electrodes are ohmic in nature and metallic layers are undamaged and conducting. The current is sent between two electrodes and voltage drop is measured across the same contacts. This measurement gives the resistance which is sum of the resistance of the bottom metallic strip plus contact resistance and the resistance of leads/wires.

**3-probe:**

After measuring 2-probe resistances, the junction resistance is measured by 3-probe measurements. This measurement gives the resistance where one voltage probe encloses one arm of the current path. This measurement allows the determination of the contact resistance.

**4-probe:**

4-probe measurements give the homogeneity of the current distribution across the junction. It is well known that in samples with non-homogenous tunnel barrier, negative resistance can be observed due to current crowding at the thinner part of the junction. In this measurement, current is sent through a metallic strip to the ferromagnetic electrode and voltage drop is measured across the other end of metallic strip and the other end of the ferromagnetic contact.

**Spin transport measurements**

The spin transport measurements are done in a local geometry as discussed earlier. The current is sent through the ferromagnet to the metallic strip and voltage is measured across it. The measurement is carried out in a transverse external magnetic field and the change in voltage is measured as a function of the field strength.

# Chapter 4: Characterization and Analysis

The characterization of the tunnel junctions fabricated by different processes starts by first measuring the current-voltage (I-V) curve both at room and low temperatures. Then the junction resistance as a function of in-plane and out of plane external magnetic field (Inverted Hanle and Hanle effect) are measured.

Various sets of 3-terminal pillar devices were prepared using different oxidation techniques. First device was fabricated with plasma oxidation for 15sec, 25 sec in an electron gun evaporator. The bottom Al layer was sputtered and it was then oxidized by plasma oxidation. After oxidation process the samples were loaded in electron gun evaporator and the FM layer was deposited along with the Au contacts without any cleaning of the oxidized samples. Second and third device were fabricated completely in sputter system where Al layer, natural oxidation (1 step oxidation and 2 step oxidation respectively) and FM layer were deposited in one step. For fourth device similar process was employed as for second and third device but processing was done in electron gun evaporator. In each device fabrication, number of samples were fabricated to maximize the yield.

Here the experimental results for the first device are discussed. The figure 4.1 shows the biasing of the device. The change in junction resistance with in-plane and out of plane external magnetic field is done with similar biased condition and also in opposite polarity.

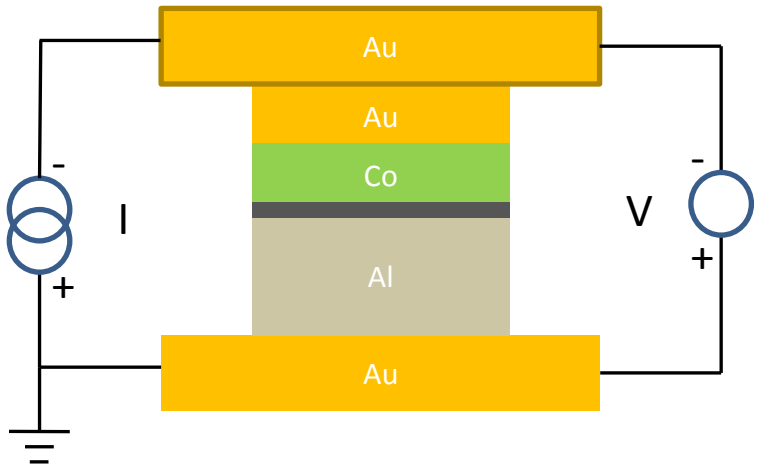


Figure 4.1: Schematic of biasing conditions used in measurements.

To get an idea of the properties of the tunnel barrier of this device, the I-V curves are fitted with Brinkman's model as described in section 2.3 of this thesis. To understand the mechanism of tunneling in a better way the I-V curves are taken at room temperature (RT) and at liquid nitrogen (77K) and liquid Helium (4K), see figure 4.2. After fitting the measured I-V curves to the Brinkman's Brinkman's model

one can obtain the thickness of tunnel barrier and the barrier potential. The Brinkman's model gives the barrier height of 3.56 $\pm$ 0.02 eV and barrier thickness of 1.31 $\pm$ 0.04nm at RT (3.77 $\pm$ 0.02 eV and 1.28 $\pm$ 0.03 nm at 77 K).

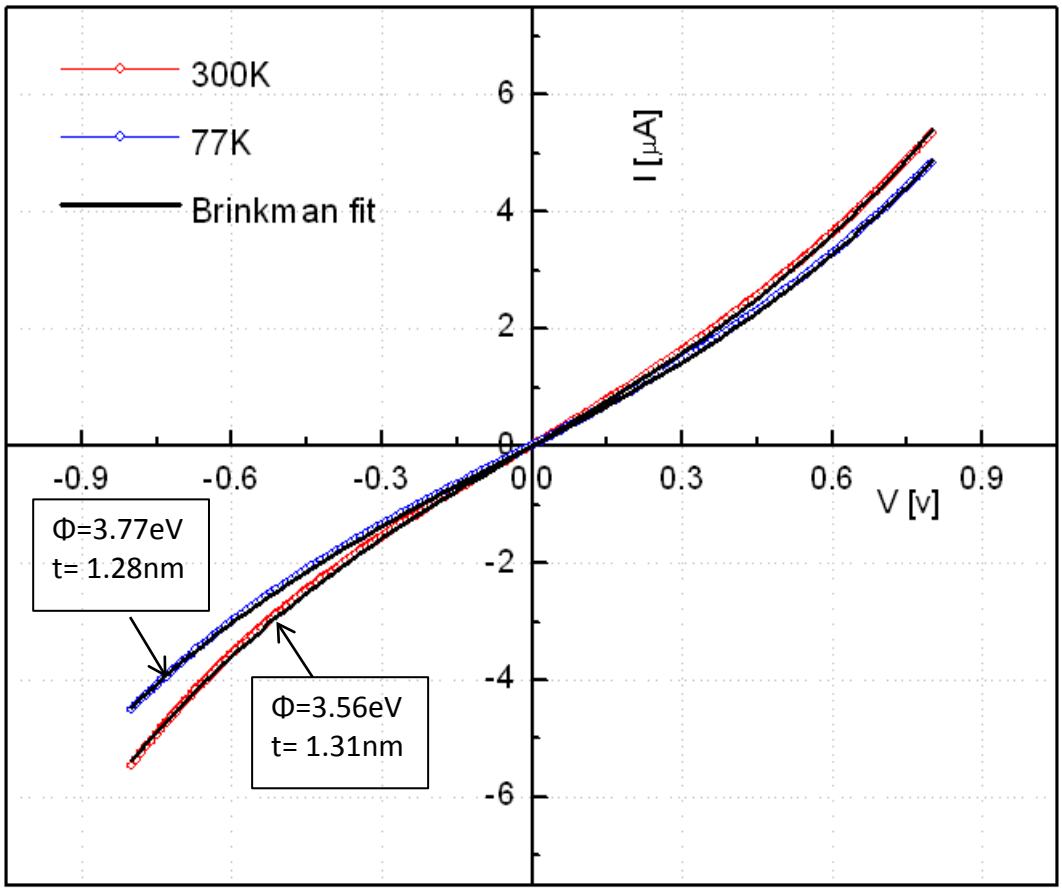


Figure 4.2: The I-V characterization of 3-terminal pillar device. I-V curves are measured at room temperature and 77K. Brinkman's model is fitted to extract the barrier height and thickness.

Figure 4.3 shows the experimental spin signals from the same device. The change in the junction resistance in the presence of out of plane external magnetic field is plotted. The measurements are done at 77 K temperature. The Lorentzian Hanle function is fitted to it to extract the spin life time. The same measurements for positive current biasing did not show any Hanle signal.

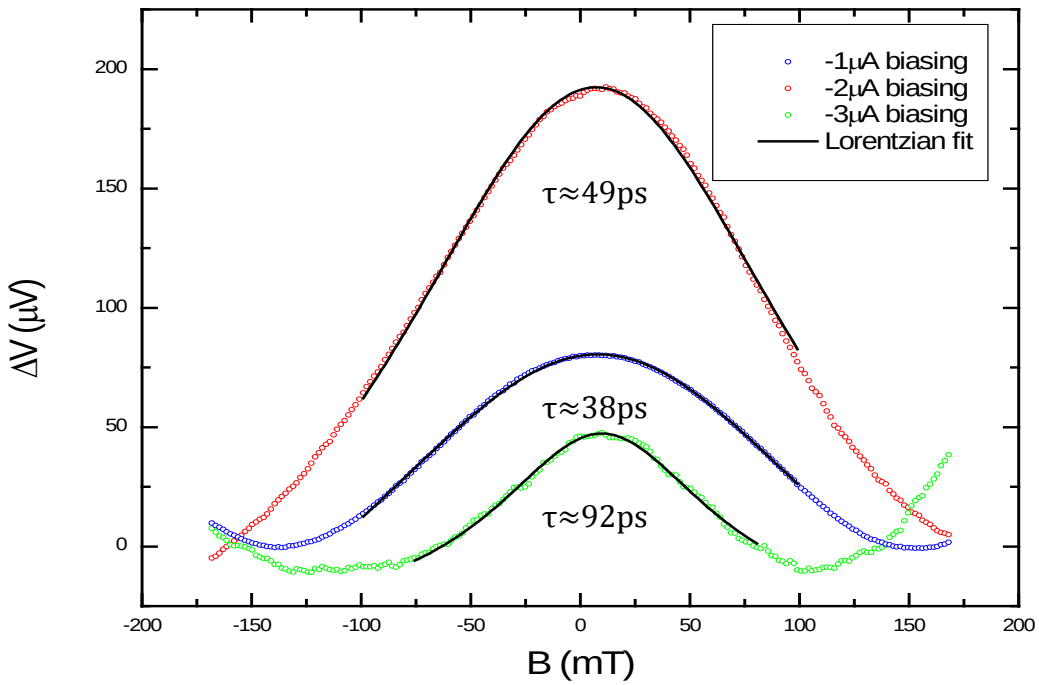


Figure 4.3: Figure shows the experimental observation of change in junction resistance as a function of out of plane external magnetic field. The observed modulation if fitted with Lorentzian function and spin life time has been extracted.

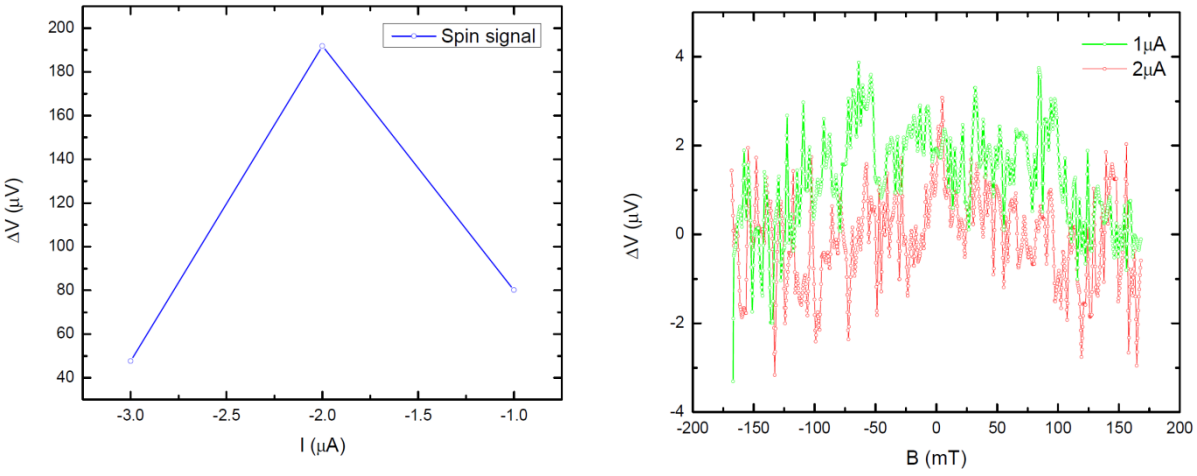


Figure4.4: a) shows the non-linear behavior of observed spin signal as a function of applied out of plane external magnetic field. (b) shows the absence of Hanle signal for positive biasing.

The non-linear scaling of the spin signal can be understood with respect to the energy dependence of the impurity states present within tunnel barrier with respect to the Fermi energy level of injecting electrode. The Hanle signal shows the spin signal of 200 Ω(for 1$\mu$A current biasing) and spin-area product (Spin RA) of $10^5$ Ω$\mu m^2$. The measured spin signal is almost 9 orders of magnitude higher than calculated by standard spin theory as shown in section 2.2 of this thesis. The extracted spin life time of 49 ps is comparable to for the spin life times of 41 ps obtained using a local spin transport

measurements at 100K. The spin life time changes with applied bias and it almost doubles at 3 $\mu$A biasing.

To compare the observed signal with the experiments performed by other research groups on similar devices, the spin RA product is compared with the $R_{int}A$ product. The measured spin RA product follows the similar dependence on $R_{int}A$ product when compared with what is being observed in references. Figure 4.4 shows the relation between Spin RA product and $R_{int}A$ product for different devices consisting of different materials and different quality of tunnel barriers. This shows that the observed scaling behavior of the measured signal with the junction resistance points to the integral role of the tunnel junction itself rather than the spin accumulation induced in the nonmagnetic channel. This universal behavior is also observed in many other 3-terminal devices with different NM materials including semiconductors and different insulating layers[29]. In our measurement, the in-plane field dependence of the junction resistance, a.k.a the inverted Hanle signal was not observed.

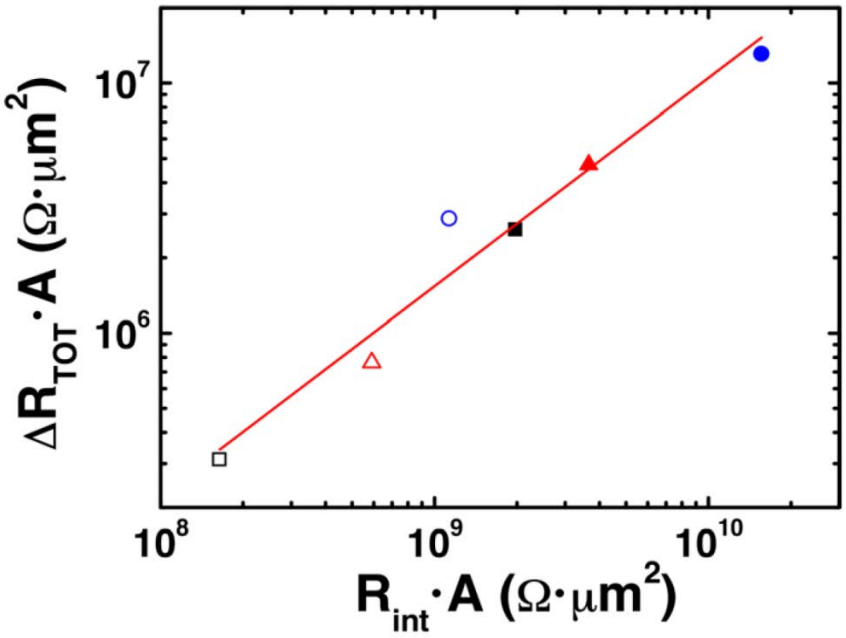


Figure 4.4: Figure adapted from[15]. Shows the dependence of the spin RA product on $R_{int}A$ product of different devices with different material and fabrication processes for the tunnel barrier. This figure suggests that the spin modulation observed in 3-terminal devices is the property of tunnel barrier.

There also exist various theories regarding this puzzling scaling behavior the spin signal with the junction resistance. Two alternative explanations center around the impurities present in the barrier. While the discusses the role of inelastic scattering through tunnel barriers, other describes the role of the on-site coulomb repulsion induced blockade on tunneling via the impurity states within the tunnel barrier.

The tunneling thorough barrier can take place by different mechanism other than direct tunneling if there are some impurity states in the tunnel barrier. Dery *et al.*[30], proposed that this tunneling through localized states depends on the number of localized states. For one localized state, electron tunnel from

one electrode to impurity state and then to other electrode. The probability of this tunneling, also known as resonant tunneling is higher for the impurity state placed at the middle of tunnel barrier width and with an energy within intrinsic width of Fermi level[31]. The resonant tunneling dominates over the direct tunneling for the barriers with larger thicknesses because with thicker barriers number of impurity states and tunneling through it, is more probable. In this process the electron-phonon interaction leads to the small temperature dependent correction in the total conductivity.

In the case of localized impurities within the tunnel barrier and for specific sets of biasing conditions and energy level alignment of the reservoir electrodes with any localized state provides additional pathways for the electron to tunnel, usually refer to as inelastic tunneling. It is difficult to identify the presence of impurities in the barrier using I-V measurements and specific types of measurements such as the inelastic electron tunneling spectroscopy needs to be performed. As discussed before, the 3-terminal device measurements are prone towards inelastic tunneling through the impurity states and the defects in the barrier. In fact, these measurements can be an alternative means to probe the existence/absence of impurities in the tunnel barrier which otherwise is difficult to probe with conventional DC I-V measurement. Therefore it is very important to know the dominant tunneling process in the measurements in order to understand the Hanle measurements better. Because of the applied bias to the junction, the inelastic tunneling pathways opens up which increases the overall conductivity of the junction. This increased conductivity is shown to be responsible for overall higher Hanle signals observed in 3-terminal local devices[17]. The inelastic tunneling spectroscopy (IETS) probes the excitation lying in impurity states inside the barrier or at electrode/barrier interface. The inelastic excitation of energy $\hbar\omega_{exc}$ can take place only if applied bias V is high enough i.e. $eV \geq \hbar\omega_{exc}$ . At this bias more pathways open up for conduction, the differential conductivity of the junction increases. The second derivative of conductivity at this applied bias shows the peak at the excitation energy.

Another possible explanation is put forward by Y.Song, H. Derry[30]and F. Casanova[16], based on the concept of the spin blockade of an electron hopping from one impurity energy level to another. The large spin accumulation signals observed in the experiments are then linked to tunneling through the impurity states with large on-site coulomb repulsion energy. In this theory the impurity sites are classified in two types based on their energetics, namely type A and type B. For the type A impurity state the energy needed to put one electron in the impurity state is within the bias limit and for type B two electrons can be put in impurity states in a applied bias regime. This is shown schematically in figure 4.5.

As shown in figure 4.5, if both type of impurities are present in a tunnel barrier under consideration, one can see the on-site coulomb repulsion. If electron tunnels from a FM electrode to type A impurity state with one particular spin then this electron cannot travel to second level of the type B impurity state if the first level is occupied by an electron of a similar spin. This can be understood with the help of Pauli principle. This results in a blockade of a steady state current across the junction. In order to remove this blockade one needs to destroy the correlation between spins in those impurity states. The spin interaction between these states can be randomized by applying an external magnetic field. If the

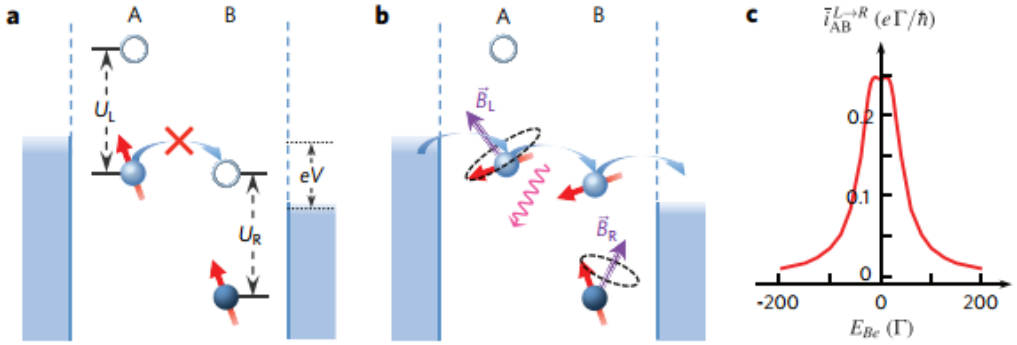


Figure 4.5: This figure is adapted from the reference[16]. (a) shows the single chain of type A and type B impurity state. Because of the blockade, the tunneling of electrons is blocked if the lower levels of impurity states of type A and type B have electrons with parallel spin. (b) shows randomization of spins in impurity states in the presence of small magnetic fields. The dominant tunneling process in these levels is phonon assisted. C) shows the simulated magneto resistance effect for such impurity states within the tunnel barrier.

external magnetic field is stronger than the magnetic interaction between the impurity states, then both impurity states experiences the same external magnetic field. But for small external magnetic field the blockade is removed as different electrons from different impurity states experience different precession and that result in the randomization of spin correlation within the tunnel junction. This behavior is shown schematically in figure 4.5b. This picture can be generalized for any longer chains of A-B impurity of the tunnel barriers with different thicknesses.

The possible explanation for not observing the Hanle signal for this device in the positive biasing can be the energy dependence of the spin polarization. As shown in figure 4.5, when negative biasing (see figure 4.1) is applied to the junction one injects the electrons from a FM to a NM and in the case of positive biasing electrons are extracted from a NM to a FM. When one injects the electron from a FM to a NM, the difference of DOS of a FM at the Fermi level for spin up and spin down electrons is increased and this can be seen with higher spin injection in to a NM. On the other hand when one extracts the electrons from NM to FM , the difference in DOS of FM at Fermi level for spin up and spin down electrons is reduced. Therefore the lesser spin injection should be observed. The fact that no Hanle signal is observed for positive bias is in agreement with this explanation.

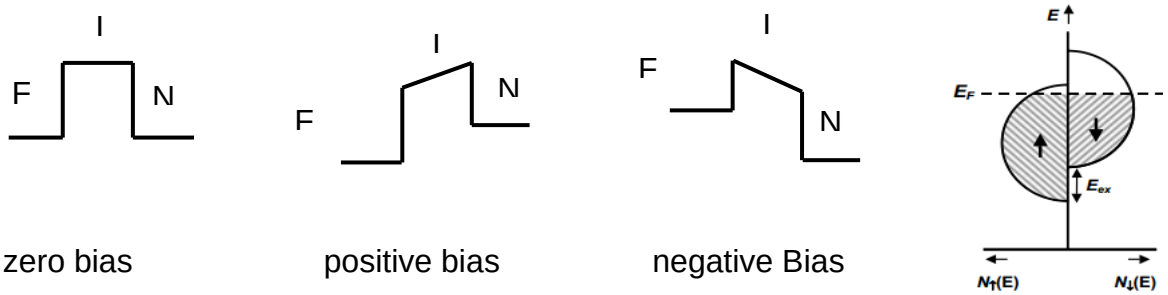


Figure4.5: Figure shows the FM-I-NM junctions under different biasing. When junction is negatively biased one injects electron from FM to NM and in opposite polarity one extracts electron from NM.

Another explanation for the absence (or very low-within noise level) of the Hanle signal at positive biased is based on the on-site coulomb repulsion model discussed earlier. Consider the similar chain of A-B type impurity in the tunnel junction. If the junction is positively biased then the current will flow from NM to FM. If now the lower level of impurity B is occupied by an electron of either spin then the higher level will be occupied by an electron with opposite spin. If lower level is occupied by spin up electron then higher level of the type B impurity will be occupied by spin down electron which can hope to the type A impurity, but then it will feel the resistance while tunneling to FM as DOS for spin down electron is lower. If we consider the case when type A impurity is in close proximity to NM, then because of the coulomb blockade there won't be any hopping of an electron to type B impurity if that level is blocked by coulomb repulsion unless the hopping electron has opposite spin to that of in lower level of type B impurity.

The other devices namely device two and three, showed similar I-V curve as the device 1. The I-V curves are again fitted with Brinkman's model. The extracted barrier height and barrier thicknesses are tabulated.

| | Barrier height (Φ) | Barrier thickness (t) |
|---|---|---|
| Device2 | 1.58 ± 0.01 eV (RT)<br>1.41 ± 0.01 eV (77 K) | 2.09 ± 0.04 nm (RT)<br>2.23 ± 0.06 nm (77 K) |
| Device3 | 1.07 ± 0.01 eV (RT)<br>0.71 ± 0.01 eV (77 K) | 2.17 ± 0.14 nm (RT)<br>2.68 ± 0.28 nm (77 K) |

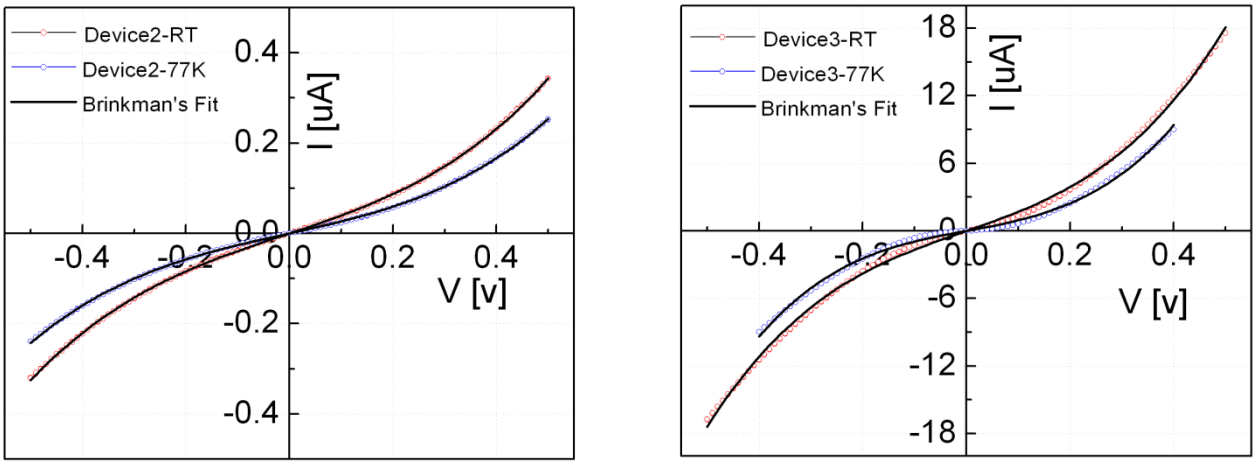


Figure 4.5: This figure shows the room temperature and 77 K, I-V curves for devices 2 and 3. The brinkman's model is fitted to extract the barrier height and the thickness.

These devices also shows some temperature dependence on the I-V curves. These devices were also studied for the Hanle and the inverted Hanle signal. These devices did not show any Hanle or inverted signal. Figure 4.6 shows the Hanle measurements performed on these devices. The plot shows some

Hanle type signal in external out of plane magnetic field but these curves do not show any bias dependence and all the curves are within noise level of experimental setup for the different biases.

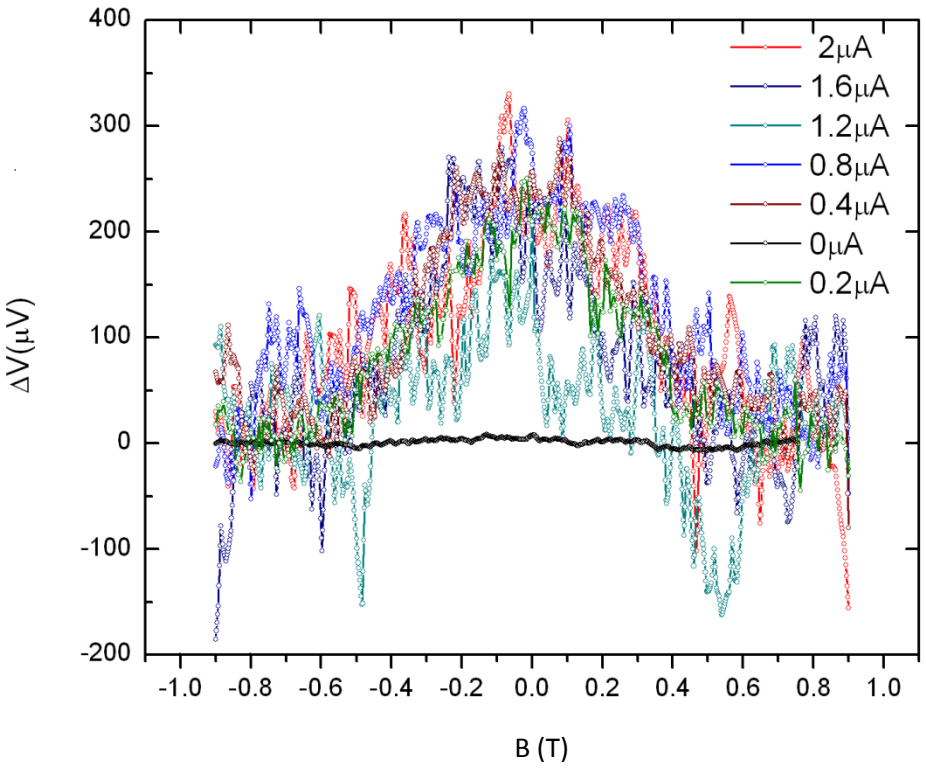


Figure4.6: This figure shows the Hanle measurements performed on the device 2. The bias dependent signal falls on each other and it's within the noise level of the experimental setup.

The possible reason for not observing any Hanle signal might be that there are no impurity states in the tunnel barrier. This is a valid possibility because for this device and also for device 3, the fabrication of the whole pillar was done in one single step. Which reduces the possibility of any contamination of the tunnel barrier. Whereas, in the first device, the pillar structure was fabricated in two steps. In first step Al layer was sputtered and then the device was loaded in electron gun evaporator for oxide formation and FM deposition, which makes the tunnel barrier prone towards the impurity.

# Conclusions:

In conclusion, the FM/I/NM 3-terminal devices were fabricated using Al as a NM and Co, Py as a FM. The properties of an insulating layer, such as tunnel barrier height, barrier thickness and temperature dependence of I-V curves, were studied. Even though not all the devices showed the expected magneto-resistance signal, well known as Hanle signal, the observed signal is 9 orders of magnitude higher than expected from the standard theory. The obtained Hanle signal does not follow the expected linear relation with the applied bias. Also the obtained signal scales with the tunnel junction resistance as observed by others[15,25], which indicates that the observed signal is dependent on the tunnel junctions. The inverted Hanle effect was not observed in any devices.

To understand the observed signal better, a theory for resonance-tunneling is employed. The finite bias on detecting electrode in the 3-terminal devices, enables the modulation of impurity driven resonance tunneling in applied external magnetic field. This modulation takes place when the Zeeman splitting of impurity states is smaller compared to applied bias. This theory can explain the observed 3-terminal spin signals without considering the spin injection and the spin relaxation in a NM systems. This also supports to the fact that the extracted spin life time from 3-terminal devices are of same order irrespective of a NM material used[14,29,32,33]. This theory also suggests that the observed modulation of the current in the presence of applied magnetic field is general effect for any impurity assisted tunneling regardless of the oxide material used and its thickness.

Since 3-terminal devices are prone towards inelastic tunneling, the inelastic tunneling spectroscopy (IETS) techniques can be employed to investigate the contribution of inelastic tunneling pathways to total current. To understand the resonance tunneling process better, more devices are need to be fabricated in a controlled manner such that tunnel barrier properties can be varied and its effect on current modulation can be studied.

# Acknowledgement :

The research presented in this thesis would have not been possible without the help and support of certain people that I would like to thank here.

First I would like to thank Prof. Bart van Wees for allowing me to work in this group and offering me a challenging but at the same time exciting project.

I would also like to thank my supervisor Fasil Dejene. You allowed me to work independently throughout this thesis project and always helped me out in all experimental and theoretical difficulties that I had. You taught me all the experimental and modelling skills required for fulfillment of this project and always kept me motivated to keep up the pace

Also I would like to thank whole metal spintronics group, Joost, Nynke and Juan, for all the help and suggestions during experiments and theoretical understanding of the concepts. Also, I would like to say thanks for all the members of Physics of Nanodevices for very pleasant stay during my thesis. I would also like to thank Martijn and Johan for all the help in the clean room difficulties.

I would like to thank all my Top masters Nanoscience cohort 2012-2014 for motivating me throughout this period to work hard and for all the discussions and suggestions over a coffee.

At the end I would express my sincere gratitude towards Zernike Institute for Advanced Materials (ZIAM) for giving me the opportunity to participate in multidisciplinary program of Top masters Nanoscience.

# References:


1. Binasch, G., Grünberg, P., Saurenbach, F. & Zinn, W. Enhanced magnetoresistance in layered magnetic structures with antiferromagnetic interlayer exchange. *Phys. Rev. B* **39,** 4828–4830 (1989).
2. Fullerton, E. E. & Schuller, I. K. The 2007 Nobel Prize in Physics: Magnetism and Transport at the Nanoscale. *ACS Nano* **1,** 384–389 (2007).
3. Wolf, S. A. *et al.* Spintronics: A Spin-Based Electronics Vision for the Future. *Science* **294,** 1488–1495 (2001).
4. Jedema, F. J., Filip, A. T. & van Wees, B. J. Electrical spin injection and accumulation at room temperature in an all-metal mesoscopic spin valve. *Nature* **410,** 345–348 (2001).
5. Mendoza, B. S. & Cabellos, J. L. Optical spin injection at semiconductor surfaces. *Phys. Rev. B* **85,** 165324 (2012).
6. Costache, M., Sladkov, M., Watts, S., van der Wal, C. & van Wees, B. Electrical Detection of Spin Pumping due to the Precessing Magnetization of a Single Ferromagnet. *Phys. Rev. Lett.* **97,** (2006).
7. Castel, V., Vlietstra, N., Youssef, J. B. & Wees, B. J. van. Platinum thickness dependence of the inverse spin-Hall voltage from spin pumping in a hybrid yttrium iron garnet/platinum system. *Appl. Phys. Lett.* **101,** 132414 (2012).
8. Valet, T. & Fert, A. Theory of the perpendicular magnetoresistance in magnetic multilayers. *Phys. Rev. B* **48,** 7099–7113 (1993).
9. Jedema, F. J. Electrical spin injection in metallic mesoscopic spin valves. at <http://irs.ub.rug.nl/ppn/244584443>
10. Schmidt, G., Ferrand, D., Molenkamp, L. W., Filip, A. T. & Van Wees, B. J. Fundamental obstacle for electrical spin injection from a ferromagnetic metal into a diffusive semiconductor. *Phys. Rev. B* **62,** R4790 (2000).
11. Fert, A. & Jaffrès, H. Conditions for efficient spin injection from a ferromagnetic metal into a semiconductor. *Phys. Rev. B* **64,** (2001).
12. Shiraishi, M. Electrically-Generated Pure Spin Current in Graphene. *Jpn. J. Appl. Phys.* **51,** 08KA01 (2012).
13. Ji, Y., Hoffmann, A., Pearson, J. E. & Bader, S. D. Enhanced spin injection polarization in Co/Cu/Co nonlocal lateral spin valves. *Appl. Phys. Lett.* **88,** 052509 (2006).

14. Casanova, F., Sharoni, A., Erekhinsky, M. & Schuller, I. Control of spin injection by direct current in lateral spin valves. *Phys. Rev. B* **79,** (2009).
15. Txoperena, O. *et al.* How reliable are Hanle measurements in metals in a three-terminal geometry? *Appl. Phys. Lett.* **102,** 192406 (2013).
16. Txoperena, O. *et al.* Universal impurity-assisted tunneling magnetoresistance under weak magnetic field. *ArXiv Prepr. ArXiv14040633* (2014). at <http://arxiv.org/abs/1404.0633>
17. Tinkey, H. N., Li, P. & Appelbaum, I. Inelastic electron tunneling spectroscopy of local' spin accumulation' devices. *ArXiv Prepr. ArXiv14052297* (2014). at <http://arxiv.org/abs/1405.2297>
18. Pifer, J. H. Microwave conductivity and conduction-electron spin-resonance linewidth of heavily doped Si: P and Si: As. *Phys. Rev. B* **12,** 4391 (1975).
19. Zarifis, V. & Castner, T. G. Observation of the conduction-electron spin resonance from metallic antimony-doped silicon. *Phys. Rev. B* **57,** 14600 (1998).
20. Gray, N. W. & Tiwari, A. Room temperature electrical injection and detection of spin polarized carriers in silicon using MgO tunnel barrier. *Appl. Phys. Lett.* **98,** 102112 (2011).
21. Vera-Marun, I. J., van Wees, B. J. & Jansen, R. Spin Heat Accumulation Induced by Tunneling from a Ferromagnet. *Phys. Rev. Lett.* **112,** (2014).
22. Slachter, A., Bakker, F. L. & van Wees, B. J. Modeling of thermal spin transport and spin-orbit effects in ferromagnetic/nonmagnetic mesoscopic devices. *Phys. Rev. B* **84,** (2011).
23. Frenkel, J. On the electrical resistance of contacts between solid conductors. *Phys. Rev.* **36,** 1604 (1930).
24. Shang, C. H., Nowak, J., Jansen, R. & Moodera, J. S. Temperature dependence of magnetoresistance and surface magnetization in ferromagnetic tunnel junctions. *Phys. Rev. B* **58,** R2917 (1998).
25. Sharma, S. Electrical creation of spin polarization in silicon devices with magnetic tunnel contacts. at <http://irs.ub.rug.nl/ppn/355569116>
26. Pu, Y. *et al.* Spin accumulation detection of FMR driven spin pumping in silicon-based metal-oxide-semiconductor heterostructures. *ArXiv Prepr. ArXiv13110965* (2013). at <http://arxiv.org/abs/1311.0965>
27. Dash, S. P., Sharma, S., Patel, R. S., de Jong, M. P. & Jansen, R. Electrical creation of spin polarization in silicon at room temperature. *Nature* **462,** 491–494 (2009).
28. Flipse, J., Bakker, F. L., Slachter, A., Dejene, F. K. & van Wees, B. J. Direct observation of the spin-dependent Peltier effect. *Nat. Nanotechnol.* **7,** 166–168 (2012).

29. Aoki, Y. *et al.* Investigation of the inverted Hanle effect in highly doped Si. *Phys. Rev. B* **86,** 081201 (2012).
30. Song, Y. & Dery, H. Magnetic Field Modulated Resonant Tunneling in Ferromagnetic-Insulator-Nonmagnetic junctions. *ArXiv14017649 Cond-Mat* (2014). at <http://arxiv.org/abs/1401.7649>
31. Xu, Y., Ephron, D. & Beasley, M. R. Directed inelastic hopping of electrons through metal-insulator-metal tunnel junctions. *Phys. Rev. B* **52,** 2843 (1995).
32. Ando, Y. *et al.* Temperature evolution of spin accumulation detected electrically in a nondegenerated silicon channel. *Phys. Rev. B* **85,** (2012).
33. Van Staa, A., Wulfhorst, J., Vogel, A., Merkt, U. & Meier, G. Spin precession in lateral all-metal spin valves: Experimental observation and theoretical description. *Phys. Rev. B* **77,** (2008).